Chemical Science

ROYAL SOCIETY OF CHEMISTRY

EDGE ARTICLE

View Article Online
View Journal | View Issue

Cite this: *Chem. Sci.*, 2025, **16**, 12455

All publication charges for this article have been paid for by the Royal Society of Chemistry

Bioorthogonal probes for L-form conversion visualization and insights into antimicrobial resistance†

Yunzhe Tao,[a] Yongwei Feng,[ba] Yu Peng,[a] Xiang Wang,[a] Xiangchuan Meng,[a] Youjun Xu,[b] Xiaowan Han,*[a] Qingyang Zhang*[a] and Hai-Yu Hu*[a]

Received 27th February 2025
Accepted 30th May 2025

DOI: 10.1039/d5sc01586c

rsc.li/chemical-science

Cell wall-deficient bacteria (CWDB) are key contributors to antimicrobial resistance (AMR), enabling persistent infections by evading antibiotics through their transition to L-form states. Therefore, molecular tools for detecting L-form conversion and AMR mechanisms are crucial for developing novel strategies against bacterial infections. Herein, we present the development of small-sized, peptidoglycan-specific fluorogenic probes employing a two-step bioorthogonal strategy that enables real-time visualization of CWDB formation. **Tz-FL-S** rapidly reacts with the novel D-alanine derivative **TCO-D-Ala** at a rate of (2.61 ± 0.07) × 10^3 M^{-1} s^{-1}, resulting in a 4.9-fold increase in fluorescence intensity. This platform exhibited excellent labeling of peptidoglycan in both Gram-positive and Gram-negative bacteria (signal-to-noise ratio: 15 to 305), effectively capturing the transition from N-form to L-form. Furthermore, we investigated the impact of 14 kinds of antibiotics on L-form conversion and found 13 of them induced CWDB. Besides, we explored the relationship between L-form conversion and AMR. This research enhances our understanding of bacterial adaptations and resistance mechanisms, paving the way for innovative strategies to combat drug-resistant infections.

Introduction

Antimicrobial resistance (AMR) has emerged as a major challenge to global public health.[1] Recent studies have identified cell wall-deficient bacteria (CWDB) as one of the key contributors to AMR,[2,3] frequently causing chronic and recurrent clinical infections.[4,5] Under survival pressures, some bacteria partially or completely lose their cell walls, converting to a cell wall-deficient (L-form) state.[6] This adaptation allowed them to evade cell wall-targeting antibiotics, such as β-lactams, making L-form bacteria resistant to many conventional treatments.[7] Moreover, research showed that CWDB could even evade phage therapy,[8–10] further complicating treatment strategies. A deeper understanding of the biological characteristics of CWDB and the molecular mechanisms underlying the transition from normal (N-form) to cell wall-deficient (L-form) bacteria—including when, why, and how this transition occurred is crucial for developing innovative antibacterial strategies and reversing the rising trend of antimicrobial resistance. Bacterial cell wall defects are typically visualized and analyzed using scanning electron microscopy (SEM) and transmission electron microscopy (TEM).[11–13] Besides, phase contrast microscopy has been also employed to observe the L-form conversion.[4,10] However, SEM and TEM are limited by complex sample preparation, high equipment costs, and the inability to visualize live bacteria, and phase contrast microscopy lacks the spatial resolution for observing peptidoglycan. In contrast, confocal laser scanning microscopy (CLSM) offers advantages such as high sensitivity and excellent spatial and temporal resolution,[14,15] making it a promising tool for monitoring the conversion of L-form bacteria in live cells. Despite the progress of AMR sensing technologies,[16–19] the development of effective fluorescent probes capable of visualizing the transition from N-form to L-form bacteria in real time remains a significant challenge. The unique structure of the bacterial cell wall, particularly the outer membrane barrier in Gram-negative bacteria, blocks the penetration of conventional fluorescent probes into live cells.[20] Therefore, developing novel probe design strategies that allow for specific and efficient labeling of both Gram-positive and Gram-negative bacterial cell walls is crucial. When combined with modern fluorescence imaging techniques, these probes would enable the real-time visualization of CWDB and the

[a]*State Key Laboratory of Bioactive Substance and Function of Natural Medicines, Institute of Materia Medica, Chinese Academy of Medical Sciences and Peking Union Medical College, Beijing, 100050, China. E-mail: hanxiaowan@imm.ac.cn; zhangqingyang@imm.ac.cn; haiyu.hu@imm.ac.cn*

[b]*School of Pharmaceutical Engineering, Key Laboratory of Structure-Based Drug Design & Discovery (Ministry of Education), Shenyang Pharmaceutical University, Shenyang, 110016, China*

† Electronic supplementary information (ESI) available: Details about abbreviations, materials and methods, synthetic procedures, compounds characterization, confocal fluorescence imaging conditions, and theoretical calculations, *etc.*; UV-vis spectra, mass spectra, additional confocal imaging data, NMR spectra. See DOI: https://doi.org/10.1039/d5sc01586c

transition from N-form to L-form, providing valuable insights into bacterial physiology and offering potential opportunities for addressing antimicrobial resistance.

Peptidoglycan (PGN), a key component of the bacterial cell envelope in both Gram-positive and Gram-negative bacteria, is essential for maintaining cell wall structural integrity.[21,22] The use of D-amino acid derivatives for metabolic labeling of bacterial peptidoglycan, as first demonstrated by Prof. Bertozzi and others, is an effective approach.[23,24] However, the labeling of peptidoglycan in Gram-negative bacteria remains a challenge because their outer membrane acts as a strong barrier that limits the entry of external compounds, including chemical probes.[25] The large size of these probes further reduces their ability to accumulate inside the cells. Consistently, studies have shown that D-alanine derivatives used for metabolic labeling have difficulty penetrating Gram-negative bacterial cells.[26,27] In this work, we developed small-sized, peptidoglycan-specific fluorogenic probes to enable real-time visualization of CWDB. Given that small-molecular-weight compounds penetrate bacterial cell walls more effectively,[27,28] we employed the two-step bioorthogonal strategy to minimize probe size (Scheme 1A). This approach deconstructed the traditional one-step fluorescent probe into two smaller components: a D-alanine *trans*-cyclooctene (TCO) derivative as an anchor and a tetrazine-tagged fluorophore. During bacterial biosynthesis, **TCO-D-Ala** metabolically incorporates at the terminus of the stem peptides in PGN,[29] while the tetrazine moiety quenches fluorescence until it undergoes a click reaction with PGN, activating the fluorophore at the bacterial cell wall and enabling no-wash fluorescence imaging. We synthesized clickable probes with various fluorophores, and after screening and optimization, **Tz-FL-S** exhibited excellent labeling of PGN, successfully capturing the transition from N-form to L-form. Furthermore, we investigated the influence of various antibiotics on L-form conversion and explored the relationship between CWDB and antimicrobial resistance. Notably, by comparing the L-form conversions of drug-susceptible and drug-resistant strains, we found that antimicrobial resistance delayed bacterial L-form conversion, likely due to the increased antibiotic tolerance of drug-resistant strains (Scheme 1B). This research provides valuable insights into bacterial physiological adaptations and resistance mechanisms, contributing to the development of new strategies to combat drug-resistant bacterial infections.

Results and discussion

Design and synthesis of probes

In designing targeted molecules derived from D-amino acids, we employed *trans*-cyclooctene as the click handle, linking it to the D-alanine structure to obtain **TCO-D-Ala**. We then synthesized a series of tetrazine-tagged clickable probes with various fluorophores: the Cy7-based probe **Tz-CY**, the naphthalimide-based

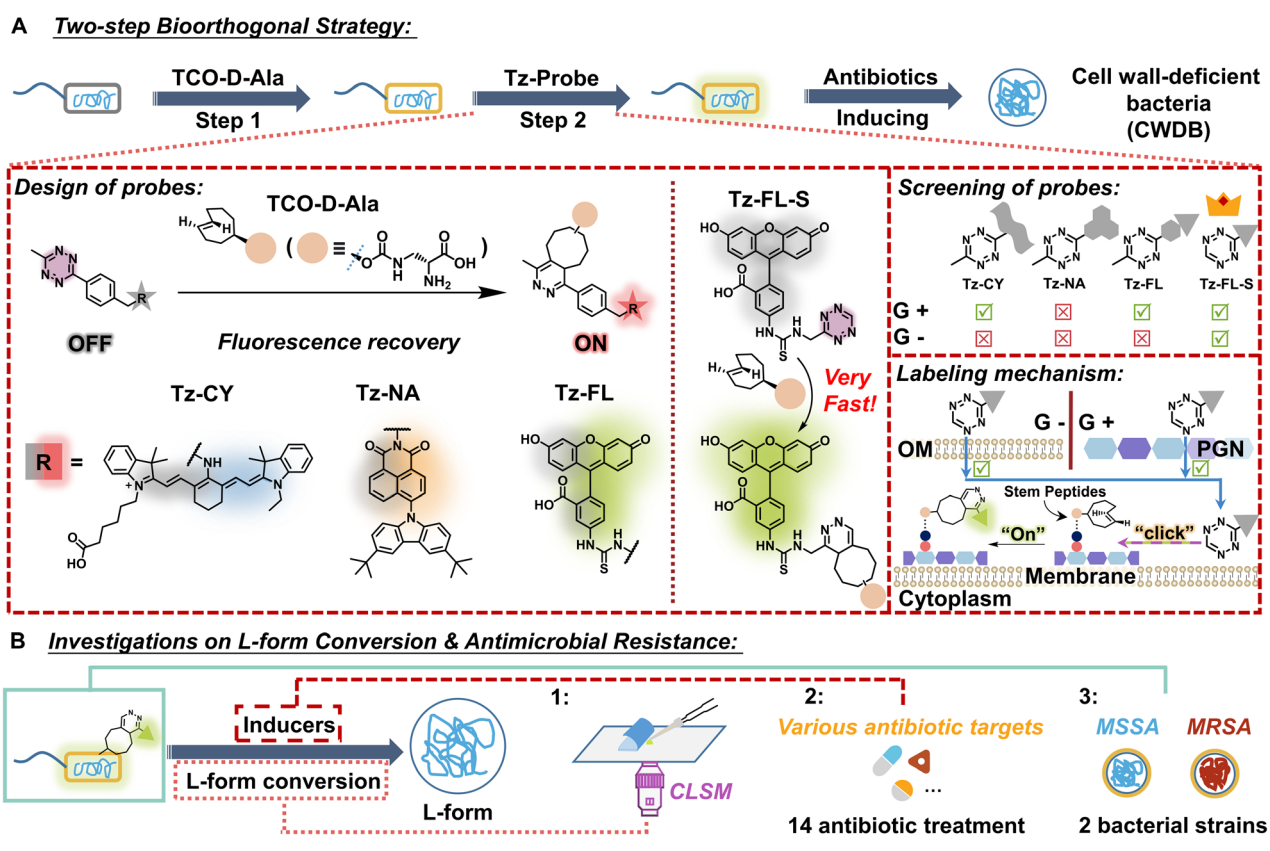

Scheme 1 Probe design and applications. (A) Design, chemical structures and sensing mechanism of TCO-D-Ala, Tz-CY, Tz-NA, Tz-FL, and Tz-FL-S in the Gram-positive and Gram-negative bacteria. (B) Tz-FL-S with TCO-D-Ala enabled visualization of L-form conversion, studies on the impact of various antibiotics on CWDB formations, and the relationship between L-form conversion and AMR.

probe **Tz-NA** and the fluorescein-based **Tz-FL**. Cyanine dye was chosen for its near-infrared (NIR) emission, which allows deeper tissue penetration and reduced background autofluorescence for *in vivo* imaging.[30] Naphthalimide–carbazole fluorophore was selected for its two-photon excitation capability and thermally activated delayed fluorescence (TADF), making it well-suited for both two-photon and time-resolved imaging.[31] Fluorescein was chosen for its high quantum yield, good water solubility, and proven biocompatibility.[32] We further reduced the molecular weight of **Tz-FL**, resulting in the development of **Tz-FL-S**, which optimized its labeling efficiency and ensured robust performance in complex biological environments.

The main synthesis is outlined in Scheme S1.† The targeted D-alanine derivative, **TCO-D-Ala**, was synthesized by reacting the active *p*-nitrophenyl esters of *trans*-cyclooctene with modified D-Ala, followed by a deprotection step. Subsequently, we synthesized the tetrazine intermediate, compound **6**, according to relevant literature.[33] Using this intermediate, we then conjugated it with cyanine, naphthalimide, and fluorescein through 1–2 substitution and coupling reactions to obtain the probes **Tz-CY**, **Tz-NA**, and **Tz-FL**, respectively. Finally, we synthesized a smaller probe, **Tz-FL-S**, using a simplified tetrazine fragment, compound **15**.[34] The detailed synthetic procedures and analytical data for the compounds are provided in the ESI.†

The "off–on" fluorescence of Tz-CY, Tz-NA, and Tz-FL

Firstly, we examined the spectral responses of **Tz-CY**, **Tz-NA**, and **Tz-FL** upon reacting with **TCO-D-Ala** in pH 7.4 phosphate-buffered saline (PBS). As shown in Fig. S1,† the absorption spectra of the three probes exhibited minimal changes after their reaction with **TCO-D-Ala**, indicating that there was no significant alteration in the chromophore structure. As expected, all three probes demonstrated a pronounced quenching effect of the tetrazine moiety on the chromophore (Fig. 1). Upon the addition of **TCO-D-Ala** in PBS, the fluorescence intensity of **Tz-CY** and **Tz-FL** increased by 7.2-fold at 764 nm and 7.4-fold at 520 nm, respectively (Fig. 1A and D). In contrast, **Tz-NA** exhibited only a slight fluorescence recovery, which could be attributed to its high lipophilicity potentially inducing aggregation in PBS, thereby diminishing its reactivity with **TCO-D-Ala** (Fig. 1B). To investigate this hypothesis, we subsequently performed a reaction between **Tz-NA** and **TCO-D-Ala** in dimethyl sulfoxide (DMSO). The results indicated a favorable reaction in this solvent, with **Tz-NA**'s fluorescence intensity recovering by up to 21-fold at 590 nm (Fig. 1C). Liquid chromatography-mass spectrometry (LC-MS) analysis further confirmed that the probes **Tz-CY**, **Tz-NA**, and **Tz-FL** could efficiently undergo bioorthogonal reactions with **TCO-D-Ala**, yielding the corresponding products.

Labeling discriminations on Gram-positive and Gram-negative bacteria

Subsequently, we employed *S. aureus* ATCC 29213, *E. coli* ATCC 25922, and *B. subtilis* ATCC 6633 as models to assess the labeling efficacy of our probes for both Gram-positive and Gram-negative bacteria.[24] The treated group was treated with 1 mM **TCO-D-Ala**, whereas the control group received no treatment with **TCO-D-Ala**. After reaching the logarithmic growth phase, bacteria were subjected to secondary labeling with **Tz-CY**, **Tz-NA**, and **Tz-FL** respectively. As shown in Fig. 1E, in the treated group, **Tz-CY** demonstrated labeling capability on Gram-positive bacteria, including *S. aureus* and *B. subtilis* (Fig. S2†); however, it failed to achieve specific labeling toward **TCO-D-Ala**, as indicated by fluorescence in the control group. This lack of specificity may be due to the predominantly negatively charged surfaces of bacteria, which attract cations and result in non-specific adsorption that hinders specific labeling of the cell wall.[35] Additionally, **Tz-CY** showed poor labeling of the Gram-negative *E. coli*, suggesting limited penetration through the outer membrane. **Tz-NA** displayed no significant labeling on any of the bacterial strains, likely due to its poor solubility (Fig. 2F). In contrast, **Tz-FL** produced bright labeling in both Gram-positive strains, but showed weak labeling effect on *E. coli* (Fig. 2G and H). Overall, our results indicate that **Tz-CY** and **Tz-**

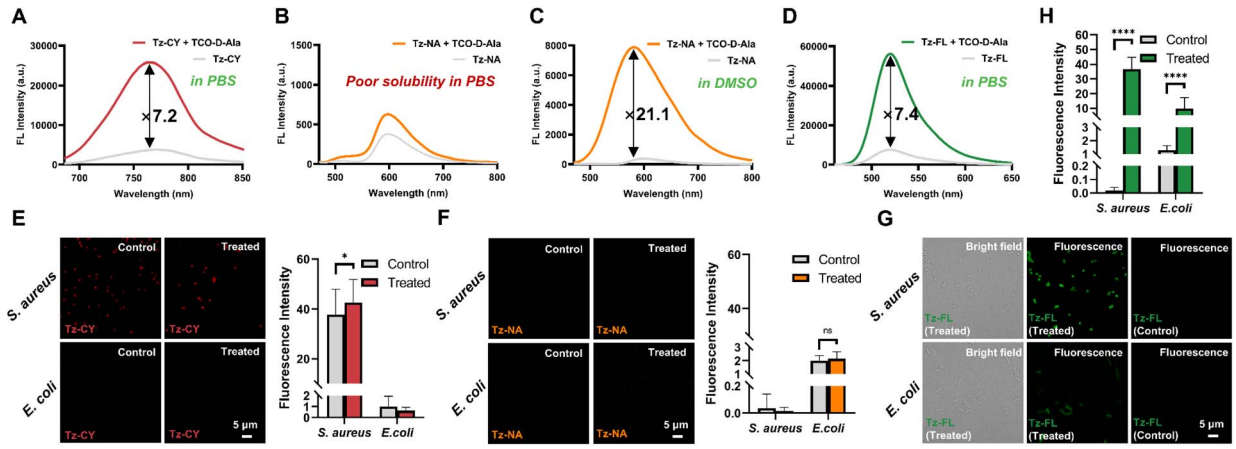

Fig. 1 The labeling properties of probes. Fluorescence spectra of **Tz-CY** (A), **Tz-NA** (B and C), and **Tz-FL** (D) before and after reacting with **TCO-D-Ala**. Fluorescence images and analysis of bacterial labeling using **Tz-CY** (E), **Tz-NA** (F), and **Tz-FL** (G and H) with (treated) or without (control) the incorporation of **TCO-D-Ala** in *S. aureus* and *E. coli*. Scale bar: 5 μm. Data are represented as mean ± SD and analyzed using a two-tailed Mann–Whitney *U* test. $n \geq 20$, ns, no significance; $P < 0.05$, ****$P < 0.0001$.

NA did not meet the expected labeling efficacy for **TCO-D-Ala** in the bacterial PGN, while the better **Tz-FL** effectively imaged Gram-positive bacteria but struggled with Gram-negative bacteria, likely due to the additional outer membrane that necessitates improved probe penetration.[36,37]

Optimized Tz-FL-S had a better performance than Tz-FL

To enhance penetration in Gram-negative bacteria, we synthesized a smaller probe, **Tz-FL-S**, using a simplified tetrazine fragment (Fig. 2A). Spectral response analysis of **Tz-FL-S** revealed similar absorbance curves before and after incubation with **TCO-D-Ala** (Fig. S3A†). Notably, the tetrazine moiety maintained a significant quenching effect on fluorescein. Following the reaction with **TCO-D-Ala**, the fluorescence intensity increased by 4.9-fold at 520 nm (Fig. 2B), and LC-MS analysis confirmed the presence of bioorthogonal products (Fig. S3B†).

To investigate the fluorescence quenching mechanism, we conducted density functional theory (DFT) and time-dependent DFT (TD-DFT) calculations on **Tz-FL** and **Tz-FL-S**. The results aligned well with the Energy Transfer to a Dark State (ETDS) quenching mechanism (Fig. S4A and B†).[38] Our calculations demonstrated that the excited-state energy transferred from the fluorophore to the tetrazine moiety, followed by internal conversion to the low-energy dark state (S_1) of tetrazine, ultimately returning to the ground state through non-radiative decay processes. The click reaction with the tetrazine group disrupted ETDS process, restoring fluorescence emission from the fluorophores. Specifically, **Tz-FL-S** exhibited a low-lying dark state (S_1) with a negligible oscillator strength ($f = 0.005$). After the reaction with **TCO-D-Ala**, photoexcitation from S_0 to S_1 was primarily driven by the $\pi \rightarrow \pi^*$ transition of the fluorophore moiety, resulting in a substantial increase in oscillator strength ($f = 0.520$). Fluorescence turn-on efficiency depended on the distance between the fluorophore and tetrazine.[38] **Tz-FL-S** had a longer distance between the fluorescein and tetrazine groups than **Tz-FL** (Fig. S4C†), which likely caused its slightly lower fluorescence recovery.

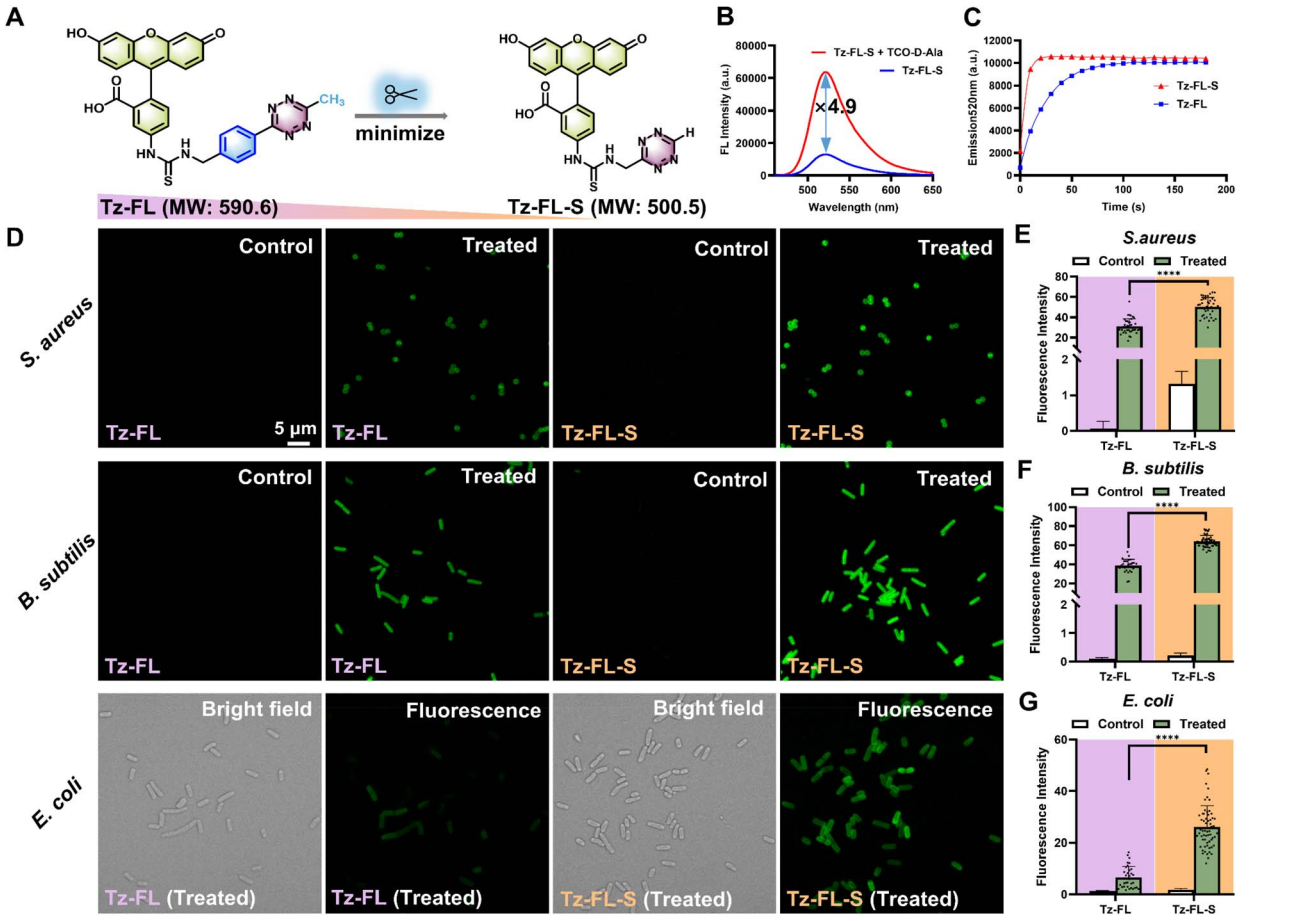

Fig. 2 Probe optimization. (A) Strategy to optimize **Tz-FL** into **Tz-FL-S** by removing the benzene ring in the linker and the methyl group from the tetrazine head. (B) Fluorescence spectra of **Tz-FL-S** before and after reacting with **TCO-D-Ala** in pH 7.4 PBS, $\lambda_{ex} = 488$ nm. (C) Plot of fluorescence intensity at 520 nm *versus* time. **Tz-FL-S** exhibited a faster reaction than **Tz-FL**. $\lambda_{ex} = 488$ nm. (D) Labeling of *S. aureus* ATCC 29213, *B. subtilis* ATCC 6633, and *E. coli* ATCC 25922 with **Tz-FL** or **Tz-FL-S**. Green fluorescence images for each strain were collected and processed under the same conditions. For Hoechst staining images in the **Tz-FL-S** group, see Fig. S3C.† Scale bar: 5 μm. (E), (F), and (G) mean fluorescence intensity of bacteria labeled by **Tz-FL** and **Tz-FL-S** from panel (D) ($n \geq 30$). Data are represented as mean ± SD and analyzed using a two-tailed Mann–Whitney *U* test. ****$P < 0.0001$.

Furthermore, we determined the reaction kinetics between **TCO-D-Ala** and either **Tz-FL** or **Tz-FL-S** by monitoring the fluorescence increase at 520 nm over time. Upon mixing the tetrazine probes with **TCO-D-Ala**, a rapid fluorescence activation was observed. The kinetic plots revealed that **Tz-FL-S** reached its fluorescence plateau within approximately 20 seconds, whereas **Tz-FL** required around 120 seconds (Fig. 2C). Curve fitting based on a pseudo-first-order reaction model (Fig. S3E and F†) yielded a rate constant of $(2.61 \pm 0.07) \times 10^3\ M^{-1}\ s^{-1}$ for **Tz-FL-S** and $(5.08 \pm 0.04) \times 10^2\ M^{-1}\ s^{-1}$ for **Tz-FL**. The corresponding half-lives $t_{1/2}$ were 3.3 ± 0.1 s for **Tz-FL-S** and 17.0 ± 0.1 s for **Tz-FL**, respectively. Thus, the reaction rate constant of **Tz-FL-S** is approximately 5.2 times higher than that of **Tz-FL**. Studies showed that the H-tetrazine reacted significantly faster than the Me-tetrazine,[39–41] and our results are consistent with this trend. More importantly, **Tz-FL-S** exhibited superior labeling capabilities for both Gram-positive and Gram-negative bacteria compared to **Tz-FL** (Fig. 2D–G). It showed strong fluorescent signals on *S. aureus* and *B. subtilis*, providing specific, brighter, and more uniform labeling for the Gram-negative bacterium *E. coli*, while the negative control displayed no obvious signal (Fig. S3D†). In Fig. 2G, for the treated *E. coli* groups, the fluorescence intensity (mean ± SD) for **Tz-FL** is 6.5 ± 4.3, and for **Tz-FL-S**, it is 26.0 ± 8.3. Uniformity was assessed using the relative standard deviation (RSD), with **Tz-FL-S** demonstrating a lower RSD value (0.3 *vs.* 0.6 for **Tz-FL**), indicating more consistent labeling. Moreover, we quantitatively analysed **TCO-D-Ala** uptake in *E. coli*, *B. subtilis*, and *S. aureus* by plotting fluorescence intensity normalized to OD_{600} against **TCO-D-Ala** concentration following **Tz-FL-S** labeling. In *E. coli*, the uptake profile displayed a saturation curve characteristic of enzyme-catalysed kinetics, suggesting that **TCO-D-Ala** likely enters the same metabolic pathway as other D-alanine derivatives *via* transpeptidases.[29,42] Fitting the data to the Michaelis–Menten model yielded a K_m value of 17 μM for *E. coli* (Fig. S3G†). The uptake data for *B. subtilis* and *S. aureus* exhibited linear relationships within the tested concentration range, suggesting that their K_m values exceed the highest concentration tested (1 mM, Fig. S3H and I†). Although exact K_m values for *B. subtilis* and *S. aureus* could not be determined, the slope of the linear fit is expected to reflect their relative catalytic efficiencies (V_{max}/K_m). Comparative analysis revealed that **TCO-D-Ala** incorporation is 4–24 times more efficient in *E. coli*. Additionally, we assessed the fluorescence stability of the clicked product formed between **TCO-D-Ala** and **Tz-FL-S**, and observed no significant decrease in fluorescence intensity after 48 hours at 30 °C (Fig. S3J†). These results indicated that, through molecule optimization, **TCO-D-Ala** and **Tz-FL-S** effectively labeled bacterial cell walls and showed strong potential for monitoring bacterial L-form conversion, leading to its selection for further studies on CWDB.

Visualizing bacterial L-form conversion process by fluorescence imaging

During L-form conversion, bacteria undergo significant morphological changes. Although phase contrast microscopy has been employed to monitor this process in some bacterial studies, changes in peptidoglycan molecules remain unclear.[10,43,44] To visualize these changes, we used **Tz-FL-S** with **TCO-D-Ala** for labeling peptidoglycan in three strains of Gram-positive bacteria (*B. subtilis*, *S. aureus* RN 4220, and ATCC 29213) and one strain of Gram-negative bacterium (*E. coli* ATCC 25922). Hoechst 33342 was also used to label nucleoids. L-form conversion was induced using established agents—penicillin G, lysozyme, lysostaphin, and fosfomycin[43,45]—and monitored with CLSM (Fig. 3A), with the conversion stages for each strain classified as early, middle, late, and very late.

In *B. subtilis* (Fig. 3B), the early stage exhibited clear labeling of the cell wall structure (green) with Hoechst 33342 staining the nucleoids (blue). As conversion advanced to the middle stage, cracks seemly appeared in the cell wall, leading to bulging, while nucleoids began to extrude. In the late stage, nucleoids exited the peptidoglycan capsule, and the cell wall nearly disappeared. Even in the absence of the cell wall, the cell membrane continued to expand, producing enlarged CWDB in the very late stage, consistent with the literature.[46] In *S. aureus* RN 4220 (Fig. 3C), the conversion process proceeded quickly, with cells displaying bulging during the middle stage before fully detaching from the cell wall to form CWDB. In contrast, *S. aureus* ATCC 29213 (Fig. 3D) underwent a more gradual reduction in peptidoglycan, evidenced by diminishing cell wall fluorescence and an increase in cell size rather than immediate bulging. For *E. coli* (Fig. 3E), the process began with cracking in the middle stage, leading to bulging and bending at the cell ends in the late stage. Eventually, nucleoids were squeezed out, resulting in CWDB formation. Interestingly, some late-stage bulges appeared empty, possibly due to vacuole formations known to occur in *E. coli*.[47] We observed that L-form conversion did not occur uniformly among individual bacteria, likely due to variations in bacterial states. Using the fluorogenic bioorthogonal probe **Tz-FL-S** in combination with **TCO-D-Ala**, our study effectively captured the temporal and spatial dynamics of key molecular events associated with cell wall loss during bacterial L-form conversion. This approach provided a more accurate and comprehensive view than previous detection methods.

CWDB formed under the induction of different antibiotics

L-form bacteria are capable of evading most cell wall-targeting antibiotics, such as β-lactams, which can contribute to antibiotic resistance. However, their response to other classes of antibiotics remains less understood.[2] To thoroughly investigate the impact of antibiotic challenges on bacterial cell walls and to assess the capacity for CWDB formation, we selected 14 antibiotics with distinct antibacterial mechanisms for testing on *S. aureus* ATCC 29213. These antibiotics target various pathways, including penicillin-binding proteins (PBPs), bacterial protein synthesis, folic acid synthesis, and the synthesis of DNA, RNA, and peptidoglycan.[48] We acquired confocal fluorescence images to visualize CWDB formation under 14 different antibiotic treatments, with representative images shown in Fig. 4, and performed quantitative fluorescence analysis (Fig. S6†). Our

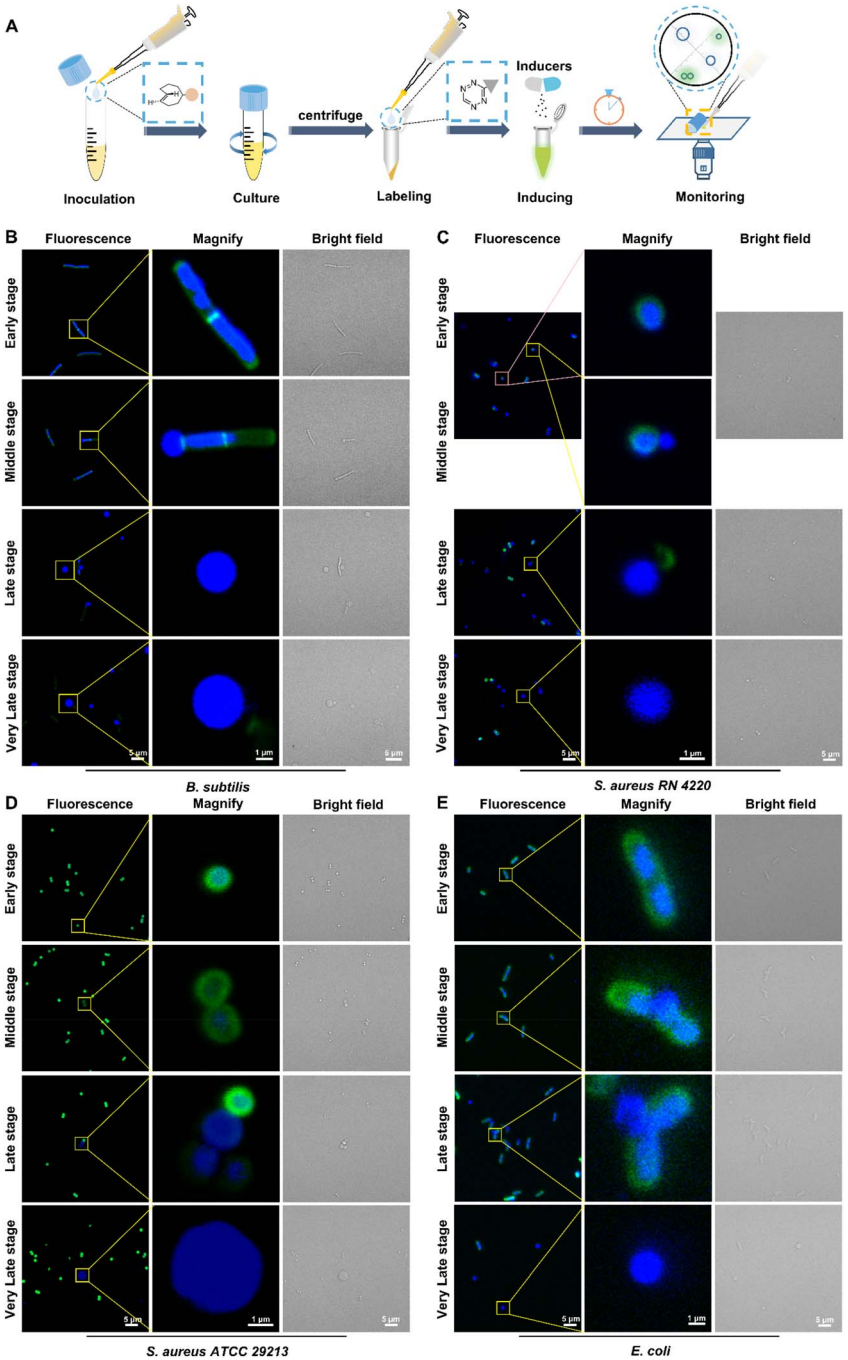

Fig. 3 Fluorescence images of different stages of bacterial L-form conversion. (A) A simplified workflow for monitoring bacterial L-form conversion. Bacteria labeled with Hoechst 33342 and **Tz-FL-S** were subjected to various induction conditions and monitored by CLSM. (B) Labeled *B. subtilis* ATCC 6633 were induced with 200 μg per mL penicillin G and 100 μg per mL lysozyme at 30 °C in NB/MSM medium. (C) Labeled *S. aureus* ATCC RN 4220 were induced with 200 μg per mL penicillin G and 2 μg per mL lysostaphin at 30 °C in NB/MSM medium. (D) Labeled *S. aureus* ATCC 29213 were induced with 400 μg per mL fosfomycin (FOS) at 30 °C in NB/MSM medium. (E) Labeled *E. coli* ATCC 25922 were induced with 100 μg per mL penicillin G and 100 μg per mL fosfomycin at 30 °C in NB/MSM medium. Scale bar: 5 μm. For the magnified images, the scale bar is 1 μm.

results demonstrate that all tested antibiotics, except vancomycin, induced CWDB formation. Treatment with fosfomycin at a concentration of 10× MIC continued to induce swollen CWDB (Fig. S5A†). For the antibiotics targeting PBPs (Fig. 4A), CWDB were observed under each treatment. Fluorescent images revealed bright green fusiform peptidoglycan shells or fragments (indicated by white arrows), which may be shed during the transition to CWDB. Upon treatment with ampicillin or penicillin G, almost all bacteria lost their cell walls and transformed into CWDB, while those treated with cefoperazone

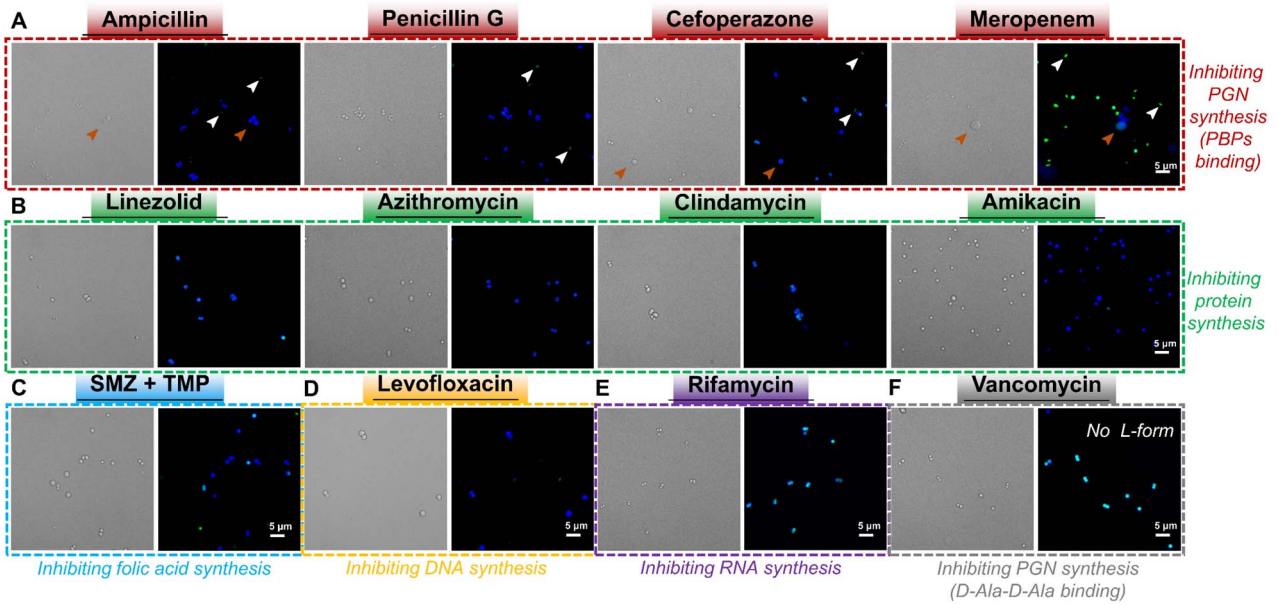

Fig. 4 Confocal fluorescence images of CWDB formation in *S. aureus* ATCC 29213 after treatment with various inducers. *S. aureus* cells were pre-labeled with Hoechst 33342 (blue) and **Tz-FL-S** (green), then exposed to antibiotics at 10× MIC in NB/MSM medium at 30 °C for 24 hours. The antibiotics inhibiting: (A) peptidoglycan synthesis *via* binding PBPs, (B) protein synthesis, (C) folic acid synthesis, (D) DNA synthesis, (E) RNA synthesis, (F) peptidoglycan synthesis *via* binding D-Ala-D-Ala terminus. White arrows indicate fusiform peptidoglycan shells or fragments, and orange arrows highlight swollen cells. SMZ: sulfamethoxazole, TMP: trimethoprim. Scale bar: 5 μm.

or meropenem retained visible, weak or strong, green fluorescence. Distinctly swollen cells were observed under ampicillin, cefoperazone, and meropenem treatment (indicated by orange arrows). Antibiotics that inhibit bacterial protein synthesis, such as linezolid, azithromycin, clindamycin, and amikacin (Fig. 4B), ultimately led to bacterial conversion into CWDB. This conversion likely occurred as these antibiotics initially bound to ribosomal subunits, directly disrupting protein synthesis and causing subsequent metabolic disturbances in the cell wall. Similarly, sulfamethoxazole (SMZ) and trimethoprim (TMP), which inhibit folic acid synthesis and thereby block nucleic acid synthesis, also prompted the majority of bacteria to become CWDB (Fig. 4C). Notably, trimethoprim alone produced a comparable effect (Fig. S5B†). Interestingly, we found that levofloxacin, which directly inhibits DNA metabolism, likely affected cell wall synthesis by hindering the transcription process and consequently blocking protein synthesis,[49] leading to CWDB formation along with the loss of the cell wall (Fig. 4D). Additionally, rifamycin, which binds to RNA polymerase to interfere with RNA synthesis,[50] likely impaired downstream protein synthesis, resulting in the formation of CWDB to some extent, as evidenced by the dim and uneven green fluorescence observed (Fig. 4E). It can be inferred that damage to the robust cell wall is a fundamental mechanism by which antibiotics induce bacterial rupture, either directly or indirectly. In studies involving vancomycin, we observed growth inhibition rather than a significant bactericidal effect, as many bacteria remained brightly labeled on their cell walls (Fig. 4F). This may be due to the extensive modification of D-Ala-D-Ala by the probes, which could hinder vancomycin binding and indirectly contribute to drug resistance.[51] As a limitation, probes based on D-alanine derivatives may not be suitable for studies involving vancomycin family drugs that bind to D-Ala-D-Ala. Nonetheless, the lack of L-form conversion observed suggests that bacteria may develop resistance to vancomycin by modifying their D-Ala-D-Ala structure, as previously reported.[52] Our findings suggest that CWDB formation can be induced not only by antibiotics that directly target the cell wall but also by those that act on other biological processes.

Antimicrobial resistance delayed the bacterial L-form conversion

Mutations that reduce drug binding to its target and increased expression of efflux pumps contribute to antibiotic resistance.[3] Additionally, tolerance, a mechanism in which non-growing or slow-growing bacteria can survive exposure to antibiotics targeting actively growing cells, highlights the complexity of antibiotic resistance.[53] To further explore the relationship between antimicrobial resistance and L-form conversion, we treated methicillin-resistant *S. aureus* (MRSA) and methicillin-susceptible *S. aureus* (MSSA) with ampicillin at 10× MIC respectively and monitored bacteria utilizing our probes (Fig. 5 and Table S1†). Although the drug-resistant strain eventually turned into CWDB, it converted more slowly than the drug-susceptible strain. From 0 h to 4 h, no obvious CWDB appeared in either strain. By 5 h, inflated CWDB completely losing their cell wall appeared in the drug-susceptible strain (yellow arrow), while just few cells in the drug-resistant strain exhibited partial loss of cell wall and inflation (orange arrow). At 7 h, the drug-susceptible strain exhibited more CWDB with lost cell wall than at 5 h (pink arrow), while the drug-resistant strain showed few CWDB, retaining a significant amount of

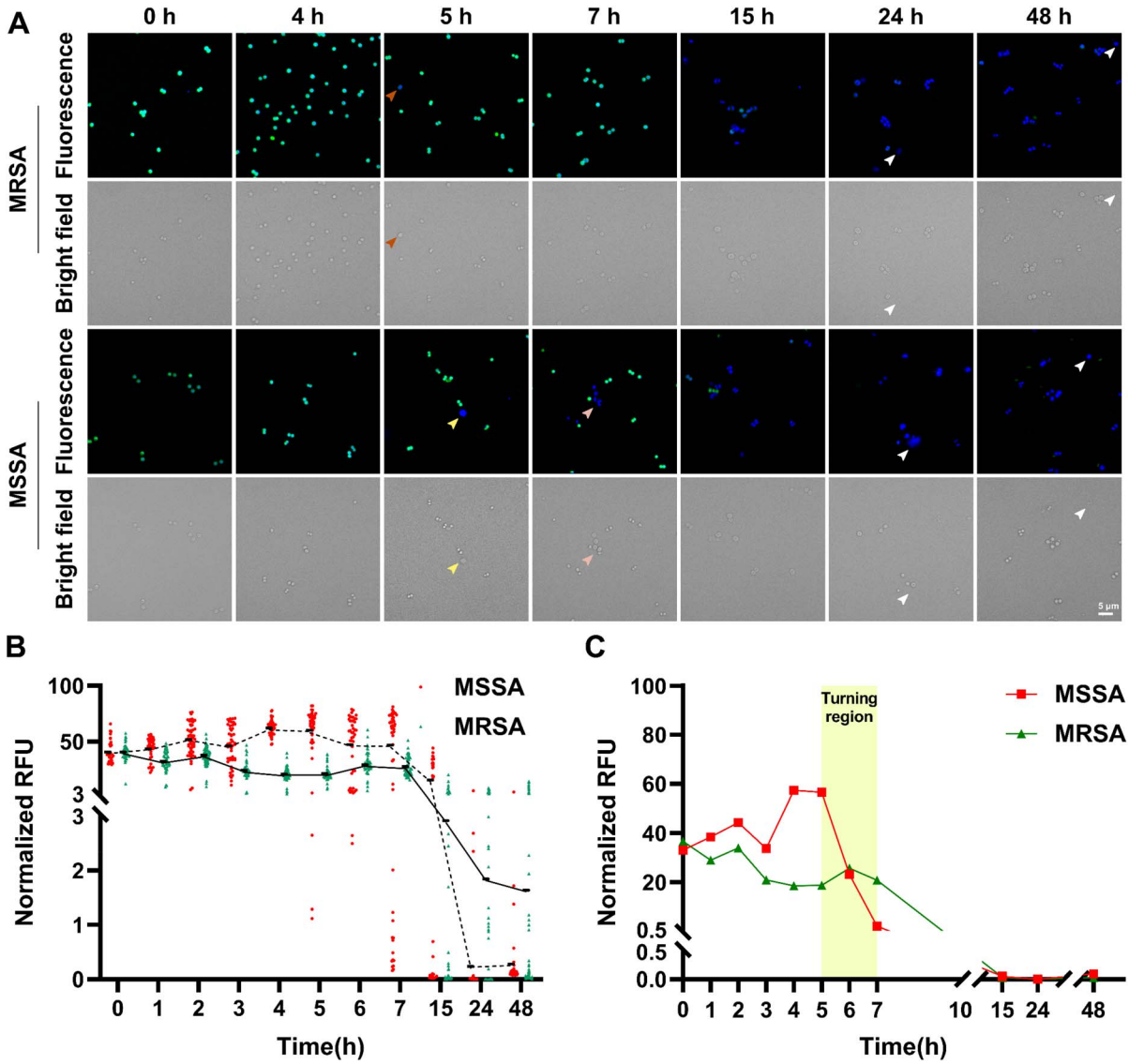

Fig. 5 Antimicrobial resistance delayed the bacterial L-form conversion. (A) Representative confocal fluorescence images of L-form conversion in Methicillin-resistant *Staphylococcus aureus* (MRSA, ATCC 33592) and Methicillin-susceptible *Staphylococcus aureus* (MSSA, ATCC 29213) induced by ampicillin. Cells were pre-labeled with Hoechst 33342 (blue) and **Tz-FL-S** (green), then induced with ampicillin at 10× MIC in NB/MSM medium at 30 °C for 48 h. Orange arrow: partial loss of cell wall in CWDB; yellow arrow: inflated CWDB with complete loss of the cell wall; pink arrow: multiple CWDB with complete loss of the cell wall; white arrow: fragile and ruptured CWDB. Scale bar: 5 μm. (B) Quantitative analysis showing the mean fluorescence intensity of individual bacteria from multiple images plotted over time. The data were normalized to ensure that the initial mean fluorescence intensity values (at 0 h) of both datasets were equivalent. (C) Plot of the first quartile (Q_1) values of mean fluorescence intensity at each time point. A distinct turning region was observed between 5 h and 7 h. RFU: relative fluorescence intensity.

peptidoglycan. By 15 h, both strains showed substantial CWDB. Additionally, at 24 h and 48 h, fragile and ruptured CWDB (white arrow) appeared, nearly invisible in the bright field but exhibiting diffuse blue fluorescence. To better illustrate the differences in L-form transition rates between resistant and susceptible strains, we quantified the mean fluorescence intensity of individual bacteria from multiple images over time. Fluorescence intensity was plotted against time (Fig. 5B), and the first quartile (Q_1) values at each time point were compared to assess the timing of CWDB formation in MSSA and MRSA (Fig. 5C). The Q_1 value represents the fluorescence intensity below which 25% of the bacterial population falls. Notably, a transition phase was observed between 5 h and 7 h, during which MRSA retained higher peptidoglycan levels and exhibited a significantly delayed conversion compared to MSSA. Despite exposure to a high antibiotic concentration, the drug-resistant bacteria took longer to exhibit conversion, suggesting that this delay may be due to antibiotic tolerance. To further investigate this, we applied a higher antibiotic concentration and slightly extended the treatment duration. When treated with a higher concentration of 50× MIC, the drug-resistant strain retained much peptidoglycan at 8 h, but eventually lost its cell wall, forming CWDB (Fig. S7A†). The conversion process can vary under different inducing conditions depending on the

strain.[43] Therefore, we further induced conversion under a solid medium condition. Under solid medium conditions at 50× MIC, the drug-resistant strain exhibited cell wall loss later than the drug-susceptible strain. At 30 h, the drug-susceptible strain converted into large, expanded CWDB (Fig. S7B†), while the drug-resistant strain only showed weakened cell wall fluorescence (Fig. S7C†). The results indicated that antimicrobial resistance delayed L-form conversion in MRSA. In our results, this delayed conversion may be attributed to the antibiotic tolerance of drug-resistant strains. These strains took longer to lose their cell walls under antibiotic exposure, regardless of the concentration used. Studies have indicated that antibiotic tolerance in *E. coli* can precede and promote antibiotic resistance.[54] However, the interaction between bacterial resistance and tolerance mutations remains underexplored. Our findings suggest potential synergistic interactions between antibiotic resistance and tolerance.[55] Nonetheless, the molecular mechanisms underlying antibiotic tolerance, especially in *S. aureus*, remain unclear. The application of fluorescent probes is anticipated to provide valuable insights into the study of bacterial tolerance.

Conclusion

CWDB, formed during the bacterial transition from the N-form to the L-form, plays a crucial role in enhancing bacterial drug resistance and viability. We employed a two-step bioorthogonal labeling strategy to design and synthesize **TCO-D-Ala**, along with a series of tetrazine-tagged, self-quenched fluorescent probes, ultimately selecting **Tz-FL-S** as the optimal probe. **TCO-D-Ala** was metabolically incorporated in bacterial peptidoglycan, and, together with **Tz-FL-S**, formed the fastest-reacting D-Ala click pair. This rapid reaction enabled bright, uniform labeling of peptidoglycan in both Gram-positive and Gram-negative bacteria, allowing us to capture peptidoglycan dynamics during L-form conversion. Moreover, our bioorthogonal probes served as highly effective sensors, enabling further investigation into bacterial L-form conversion and its relationship with antimicrobial resistance. We discovered that nearly all antibiotics disrupting peptidoglycan homeostasis—whether directly or indirectly—can induce CWDB to varying degrees. Additionally, we observed that antimicrobial resistance delayed bacterial L-form conversion, likely due to the enhanced tolerance of drug-resistant strains. These findings provide valuable insights into the patterns of bacterial L-form conversion and the underlying mechanisms of antimicrobial resistance, advancing global efforts to combat bacterial infections. Together, our probes offer powerful tools for imaging peptidoglycan dynamics, investigating antimicrobial resistance, and studying bacterial adaptation. These tools hold significant potential for advancing microbiological resistance studies, diagnostics, and therapeutic strategies.

Abbreviations

AMR	Antimicrobial Resistance
ATCC	American Type Culture Collection
B. subtilis	*Bacillus subtilis*
CLSM	Confocal Laser Scanning Microscopy
CWDB	Cell Wall-Deficient Bacteria
D-Ala	D-Alanine
DFT	Density Functional Theory
DMSO	Dimethyl Sulfoxide
DNA	Deoxyribonucleic Acid
E. coli	*Escherichia coli*
ETDS	Energy Transfer to a Dark State
FOS	Fosfomycin
LC-MS	Liquid Chromatography-Mass Spectrometry
MRSA	Methicillin-Resistant *Staphylococcus aureus*
MSM	Magnesium-Sucrose-Maleic Acid
MSSA	Methicillin-Susceptible *Staphylococcus aureus*
NB	Nutrient Broth
NIR	Near-Infrared
NMR	Nuclear Magnetic Resonance
OD	Optical Density
PBPs	Penicillin-Binding Proteins
PBS	Phosphate-Buffered Saline
PGN	Peptidoglycan
RFU	Relative Fluorescence Intensity
RNA	Ribonucleic Acid
RSD	Relative Standard Deviation
S. aureus	*Staphylococcus aureus*
SEM	Scanning Electron Microscopy
SD	Standard Deviation
SMZ	Sulfamethoxazole
TADF	Thermally Activated Delayed Fluorescence
TCO	*trans*-Cyclooctene
TD-DFT	Time-Dependent Density Functional Theory
TEM	Transmission Electron Microscopy
TMP	Trimethoprim

Data availability

The data are available in the ESI† or upon request from the authors.

Author contributions

Yunzhe Tao: investigation, methodology, formal analysis, writing – original draft, Yongwei Feng: investigation, writing – original draft, Yu Peng: software, writing – original draft, Xiang Wang: software, writing – original draft, Xiangchuan Meng: investigation, writing – original draft, Youjun Xu: writing – review and editing, Xiaowan Han: methodology, writing – review and editing, Qingyang Zhang: methodology, writing – review and editing, Hai-Yu Hu: conceptualization, supervision, writing – review and editing.

Conflicts of interest

There are no conflicts to declare.

Acknowledgements

We acknowledge Dr Yuansheng Sun and Dr Hailin Qiu from ISS for assistance with confocal imaging experiments and data analyses. We also thank Dr Luping Liu, Dr Guang Li, Dr Licheng Yang and Dr Tiantai Zhang from IMM for their insightful discussions and generous support in providing space and equipment. And we thank the IMM Network and Information Center for the assistance of theoretical calculations, especially Dr Yue Zhou and Dr Xueshi Mao. This work was partially supported by the National Natural Science Foundation of China (NSFC) projects (Grant 22477139, 22277143, and 82473886), Beijing Natural Science Foundation (2242025) and CAMS Innovation Fund for Medical Sciences (CIFMS) (Grant 2021-I2M-1-054).

References

1 C. S. Ho, C. T. H. Wong, T. T. Aung, R. Lakshminarayanan, J. S. Mehta, S. Rauz, A. McNally, B. Kintses, S. J. Peacock, C. D. L. Fuente-Nunez, R. E. W. Hancock and D. S. J. Ting, Antimicrobial Resistance: A Concise Update, *Lancet Microbe*, 2024, 100947.

2 J. J. Lazenby, E. S. Li and C. B. Whitchurch, Cell Wall Deficiency – an Alternate Bacterial Lifestyle?, *Microbiology*, 2022, **168**(8), 1218.

3 E. M. Darby, E. Trampari, P. Siasat, M. S. Gaya, I. Alav, M. A. Webber and J. M. A. Blair, Molecular Mechanisms of Antibiotic Resistance Revisited, *Nat. Rev. Microbiol.*, 2023, **21**(5), 280–295.

4 K. M. Mickiewicz, Y. Kawai, L. Drage, M. C. Gomes, F. Davison, R. Pickard, J. Hall, S. Mostowy, P. D. Aldridge and J. Errington, Possible Role of L-Form Switching in Recurrent Urinary Tract Infection, *Nat. Commun.*, 2019, **10**(1), 4379.

5 J. Errington, K. Mickiewicz, Y. Kawai and L. J. Wu, L-Form Bacteria, Chronic Diseases and the Origins of Life, *Philos. Trans. R. Soc., B*, 2016, **371**(1707), 20150494.

6 D. Claessen and J. Errington, Cell Wall Deficiency as a Coping Strategy for Stress, *Trends Microbiol.*, 2019, **27**(12), 1025–1033.

7 L. G. Monahan, L. Turnbull, S. R. Osvath, D. Birch, I. G. Charles and C. B. Whitchurch, Rapid Conversion of Pseudomonas Aeruginosa to a Spherical Cell Morphotype Facilitates Tolerance to Carbapenems and Penicillins but Increases Susceptibility to Antimicrobial Peptides, *Antimicrob. Agents Chemother.*, 2014, **58**(4), 1956–1962.

8 V. Ongenae, A. S. Mabrouk, M. Crooijmans, D. Rozen, A. Briegel and D. Claessen, Reversible Bacteriophage Resistance by Shedding the Bacterial Cell Wall, *Open Biol. J.*, 2022, **12**(6), 210379.

9 A. Petrovic Fabijan, D. Martinez-Martin, C. Venturini, K. Mickiewicz, N. Flores-Rodriguez, J. Errington and J. Iredell, L-Form Switching in Escherichia Coli as a Common β-Lactam Resistance Mechanism, *Microbiol. Spectr.*, 2022, **10**(5), e02419–e02422.

10 J. C. Wohlfarth, M. Feldmüller, A. Schneller, S. Kilcher, M. Burkolter, S. Meile, M. Pilhofer, M. Schuppler and M. J. Loessner, L-Form Conversion in Gram-Positive Bacteria Enables Escape from Phage Infection, *Nat. Microbiol.*, 2023, **8**(3), 387–399.

11 G. Slavchev, L. Michailova and N. Markova, L-Form Transformation Phenomenon in *Mycobacterium Tuberculosis* Associated with Drug Tolerance to Ethambutol, *Int. J. Microbiol.*, 2016, **5**(4), 454–459.

12 J. J. Jackson and H. Kropp, Differences in Mode of Action of (β-Lactam Antibiotics Influence Morphology), LPS Release and in Vivo Antibiotic Efficacy, *J. Endotoxin Res.*, 1996, **3**(3), 201–218.

13 Y. Sumita, M. Fukasawa and T. Okuda, Comparison of Two Carbapenems, SM-7338 and Imipenem. Affinities for Penicillin-Binding Proteins and Morphological Changes, *J. Antibiot.*, 1990, **43**(3), 314–320.

14 S. W. Paddock, Principles and Practices of Laser Scanning Confocal Microscopy, *Mol. Biotechnol.*, 2000, **16**(2), 127–149.

15 S. W. Paddock, Confocal Laser Scanning Microscopy, *BioTechniques*, 1999, **27**(5), 992–1004.

16 K. J. Fitzpatrick, H. J. Rohlf, T. D. Sutherland, K. M. Koo, S. Beckett, W. O. Okelo, A. L. Keyburn, B. S. Morgan, B. Drigo, M. Trau, E. Donner, S. P. Djordjevic and P. J. De Barro, Progressing Antimicrobial Resistance Sensing Technologies across Human, Animal, and Environmental Health Domains, *ACS Sens.*, 2021, **6**(12), 4283–4296.

17 N. Qin, P. Zhao, E. A. Ho, G. Xin and C. L. Ren, Microfluidic Technology for Antibacterial Resistance Study and Antibiotic Susceptibility Testing: Review and Perspective, *ACS Sens.*, 2021, **6**(1), 3–21.

18 R. B. P, B. G. Prajapati, R. Rajeshkumar, V. Balasubramaniam and S. Ponnusankar, Revolutionizing Antibacterial Strategies: Lipid Nanoparticles as Game-Changers in Combatting Multi-Drug-Resistant Infections, *Curr. Med. Chem.*, 2024, **32**(8), 1488–1506.

19 K. Jani, S. Mehta, R. Patel, B. Prajapati and G. Patel, Focused Insights into Liposomal Nanotherapeutics for Antimicrobial Treatment, *Curr. Med. Chem.*, 2024, DOI: **10.2174/0109298673322058241003073312**.

20 A. M. Stoorza and A. S. Duerfeldt, Guiding the Way: Traditional Medicinal Chemistry Inspiration for Rational Gram-Negative Drug Design, *J. Med. Chem.*, 2024, **67**(1), 65–80.

21 W. Vollmer, D. Blanot and M. A. De Pedro, Peptidoglycan Structure and Architecture, *FEMS Microbiol. Rev.*, 2008, **32**(2), 149–167.

22 A. J. F. Egan, J. Errington and W. Vollmer, Regulation of Peptidoglycan Synthesis and Remodelling, *Nat. Rev. Microbiol.*, 2020, **18**(8), 446–460.

23 M. S. Siegrist, S. Whiteside, J. C. Jewett, A. Aditham, F. Cava and C. R. Bertozzi, D-Amino Acid Chemical Reporters Reveal Peptidoglycan Dynamics of an Intracellular Pathogen, *ACS Chem. Biol.*, 2013, **8**(3), 500–505.

24 E. Kuru, H. V. Hughes, P. J. Brown, E. Hall, S. Tekkam, F. Cava, M. A. de Pedro, Y. V. Brun and M. S. VanNieuwenhze, In Situ Probing of Newly

Synthesized Peptidoglycan in Live Bacteria with Fluorescent D-Amino Acids, *Angew. Chem., Int. Ed.*, 2012, **51**(50), 12519–12523.

25 D. Saxena, R. Maitra, R. Bormon, M. Czekanska, J. Meiers, A. Titz, S. Verma and S. Chopra, Tackling the Outer Membrane: Facilitating Compound Entry into Gram-Negative Bacterial Pathogens, *npj Aantimicrob. Resist.*, 2023, **1**(1), 1–22.

26 Y.-P. Hsu, J. Rittichier, E. Kuru, J. Yablonowski, E. Pasciak, S. Tekkam, E. Hall, B. Murphy, T. K. Lee, E. C. Garner, K. Casey Huang, Y. V. Brun and M. S. VanNieuwenhze, Full Color Palette of Fluorescent d -Amino Acids for in Situ Labeling of Bacterial Cell Walls, *Chem. Sci.*, 2017, **8**(9), 6313–6321.

27 J. M. Fura, D. Kearns and M. M. Pires, D-Amino Acid Probes for Penicillin Binding Protein-Based Bacterial Surface Labeling*, *J. Biol. Chem.*, 2015, **290**(51), 30540–30550.

28 Y. Zheng, X. Zhu, M. Jiang, F. Cao, Q. You and X. Chen, Development and Applications of D-Amino Acid Derivatives-Based Metabolic Labeling of Bacterial Peptidoglycan, *Angew. Chem., Int. Ed.*, 2024, **63**(17), e202319400.

29 E. Kuru, A. Radkov, X. Meng, A. Egan, L. Alvarez, A. Dowson, G. Booher, E. Breukink, D. I. Roper, F. Cava, W. Vollmer, Y. Brun and M. S. VanNieuwenhze, Mechanisms of Incorporation for D-Amino Acid Probes That Target Peptidoglycan Biosynthesis, *ACS Chem. Biol.*, 2019, **14**(12), 2745–2756.

30 Y. Li, Y. Zhou, X. Yue and Z. Dai, Cyanine Conjugate-based Biomedical Imaging Probes, *Adv. Healthcare Mater.*, 2020, **9**(22), 2001327.

31 X. Wang, G. Shi, S. Xu, Y. Sun, H. Qiu, Q. Wang, X. Han, Q. Zhang, T. Zhang and H.-Y. Hu, Unravelling Immune-Inflammatory Responses and Lysosomal Adaptation: Insights from Two-Photon Excited Delayed Fluorescence Imaging, *Adv. Healthcare Mater.*, 2024, **13**(15), 2304223.

32 L. D. Lavis, Teaching Old Dyes New Tricks: Biological Probes Built from Fluoresceins and Rhodamines, *Annu. Rev. Biochem.*, 2017, **86**, 825–843.

33 A. J. C. Sarris, T. Hansen, M. A. R. de Geus, E. Maurits, W. Doelman, H. S. Overkleeft, J. D. C. Codée, D. V. Filippov and S. I. van Kasteren, Fast and pH-Independent Elimination of *Trans* -Cyclooctene by Using Aminoethyl-Functionalized Tetrazines, *Chem.–Eur. J.*, 2018, **24**(68), 18075–18081.

34 Y. Li, S. Wang, Y. Chen, M. Li, X. Dong, H. C. Hang and T. Peng, Site-Specific Chemical Fatty-Acylation for Gain-of-Function Analysis of Protein *S* -Palmitoylation in Live Cells, *Chem. Commun.*, 2020, **56**(89), 13880–13883.

35 Y. H. An and R. J. Friedman, Concise Review of Mechanisms of Bacterial Adhesion to Biomaterial Surfaces, *J. Biomed. Mater. Res.*, 1998, **43**(3), 338–348.

36 A. H. Delcour, Outer Membrane Permeability and Antibiotic Resistance, *Biochim. Biophys. Acta, Proteins Proteomics*, 2009, **1794**(5), 808–816.

37 G. M. Decad and H. Nikaido, Outer Membrane of Gram-Negative Bacteria. XII. Molecular-Sieving Function of Cell Wall, *J. Bacteriol.*, 1976, **128**(1), 325.

38 W. Chi, L. Huang, C. Wang, D. Tan, Z. Xu and X. Liu, A Unified Fluorescence Quenching Mechanism of Tetrazine-Based Fluorogenic Dyes: Energy Transfer to a Dark State, *Mater. Chem. Front.*, 2021, **5**(18), 7012–7021.

39 G. Beliu, A. J. Kurz, A. C. Kuhlemann, L. Behringer-Pliess, M. Meub, N. Wolf, J. Seibel, Z.-D. Shi, M. Schnermann, J. B. Grimm, L. D. Lavis, S. Doose and M. Sauer, Bioorthogonal Labeling with Tetrazine-Dyes for Super-Resolution Microscopy, *Commun. Biol.*, 2019, **2**(1), 1–13.

40 M. R. Karver, R. Weissleder and S. A. Hilderbrand, Synthesis and Evaluation of a Series of 1,2,4,5-Tetrazines for Bioorthogonal Conjugation, *Bioconjugate Chem.*, 2011, **22**(11), 2263–2270.

41 J. A. Wagner, D. Mercadante, I. Nikić, E. A. Lemke and F. Gräter, Origin of Orthogonality of Strain-Promoted Click Reactions, *Chem.–Eur. J.*, 2015, **21**(35), 12431–12435.

42 A. Bandyopadhyay, S. Cambray and J. Gao, Fast Diazaborine Formation of Semicarbazide Enables Facile Labeling of Bacterial Pathogens, *J. Am. Chem. Soc.*, 2017, **139**(2), 871–878.

43 Y. Kawai, K. Mickiewicz and J. Errington, Lysozyme Counteracts β-Lactam Antibiotics by Promoting the Emergence of L-Form Bacteria, *Cell*, 2018, **172**(5), 1038–1049.

44 M. Leaver, P. Domínguez-Cuevas, J. M. Coxhead, R. A. Daniel and J. Errington, Life without a Wall or Division Machine in Bacillus Subtilis, *Nature*, 2009, **457**(7231), 849–853.

45 R. Mercier, Y. Kawai and J. Errington, General Principles for the Formation and Proliferation of a Wall-Free (L-Form) State in Bacteria, *eLife*, 2014, **3**, e04629.

46 P. Domínguez-Cuevas, R. Mercier, M. Leaver, Y. Kawai and J. Errington, The Rod to L-Form Transition of Bacillus Subtilis Is Limited by a Requirement for the Protoplast to Escape from the Cell Wall Sacculus, *Mol. Microbiol.*, 2012, **83**(1), 52–66.

47 S. Takahashi, M. Mizuma, S. Kami and H. Nishida, Species-Dependent Protoplast Enlargement Involves Different Types of Vacuole Generation in Bacteria, *Sci. Rep.*, 2020, **10**(1), 8832.

48 M. A. Kohanski, D. J. Dwyer and J. J. Collins, How Antibiotics Kill Bacteria: From Targets to Networks, *Nat. Rev. Microbiol.*, 2010, **8**(6), 423–435.

49 N. G. Bush, I. Diez-Santos, L. R. Abbott and A. Maxwell, Quinolones: Mechanism, Lethality and Their Contributions to Antibiotic Resistance, *Molecules*, 2020, **25**(23), 5662.

50 R. A. Adams, G. Leon, N. M. Miller, S. P. Reyes, C. H. Thantrong, A. M. Thokkadam, A. S. Lemma, D. M. Sivaloganathan, X. Wan and M. P. Brynildsen, Rifamycin Antibiotics and the Mechanisms of Their Failure, *J. Antibiot.*, 2021, **74**(11), 786–798.

51 D. H. Williams and B. Bardsley, The Vancomycin Group of Antibiotics and the Fight against Resistant Bacteria, *Angew. Chem., Int. Ed.*, 1999, **38**(9), 1172–1193.

52 P. J. Stogios and A. Savchenko, Molecular Mechanisms of Vancomycin Resistance, *Protein Sci.*, 2020, **29**(3), 654–669.
53 A. Brauner, O. Fridman, O. Gefen and N. Q. Balaban, Distinguishing between Resistance, Tolerance and Persistence to Antibiotic Treatment, *Nat. Rev. Microbiol.*, 2016, **14**(5), 320–330.
54 I. Levin-Reisman, I. Ronin, O. Gefen, I. Braniss, N. Shoresh and N. Q. Balaban, Antibiotic Tolerance Facilitates the Evolution of Resistance, *Science*, 2017, **355**(6327), 826–830.
55 I. Levin-Reisman, A. Brauner, I. Ronin and N. Q. Balaban, Epistasis between Antibiotic Tolerance, Persistence, and Resistance Mutations, *Proc. Natl. Acad. Sci. U. S. A.*, 2019, **116**(29), 14734–14739.